

1 Skilful probabilistic predictions of UK
2 floods months ahead using machine
3 learning models trained on multimodel
4 ensemble climate forecasts

5 Simon Moulds^{1,2*}, Louise Slater², Louise Arnal³, Andy Wood^{4,5}

6 ¹ School of GeoSciences, University of Edinburgh, UK [@simmoulds].

7 ² School of Geography and the Environment, University of Oxford, UK.

8 ³ Ouranos, Montreal, Canada

9 ⁴ Climate and Global Dynamics, National Center for Atmospheric Research, Boulder, CO,
10 USA

11 ⁵ Department of Civil and Environmental Engineering, Colorado School of Mines, Golden,
12 CO, USA

13 * Corresponding author email: simon.moulds@ed.ac.uk

14 *This EarthArXiv original preprint has been submitted to Hydrology and Earth System Science*
15 *(HESS) and has not been peer-reviewed or edited.*

16

17 **Abstract**

18 Seasonal streamflow forecasts are an important component of flood risk
19 management. Hybrid forecasting methods that predict seasonal streamflow using machine
20 learning models driven by climate model outputs are currently underexplored, yet have
21 some important advantages over traditional approaches using hydrological models. Here we
22 develop a hybrid subseasonal to seasonal streamflow forecasting system to predict the
23 monthly maximum daily streamflow up to four months ahead. We train a random forest
24 machine learning model on dynamical precipitation and temperature forecasts from a
25 multimodel ensemble of 196 members (eight seasonal climate forecast models) from the
26 Copernicus Climate Change Service (C3S) to produce probabilistic hindcasts for 579 stations
27 across the UK for the period 2004-2016, with up to four months lead time. We show that
28 multi-site ML models trained on pooled catchment data together with static catchment
29 attributes are significantly more skilful compared to single-site ML models trained on data
30 from each catchment individually. Considering all initialization months, 60% of stations
31 show positive skill ($CRPSS > 0$) relative to climatological reference forecasts in the first month
32 after initialization. This falls to 41% in the second month, 38% in the third month and 33% in
33 the fourth month.

34 **1 Introduction**

35 Reliable streamflow forecasts weeks to months ahead are vital for managing the
36 impacts of hydrological variability and extremes. Dynamical subseasonal to seasonal (S2S)
37 streamflow forecasts are commonly produced by forcing a conceptual or physics-based
38 hydrological model with the outputs of dynamical seasonal forecasts from climate models,
39 and may also include a subsequent statistical or machine learning post-processing step. This
40 may be achieved either directly or indirectly – e.g., by using dynamical climate prediction
41 information as direct inputs to the hydrological model, or by using the dynamic predictions
42 or empirical information as conditioning factors in a statistical weather generation scheme
43 to create the model's input meteorological forecasts. These systems represent the current
44 standard in S2S streamflow forecasting, underpinning flood forecasting services in Europe
45 (Arheimer et al., 2020; Arnal et al., 2018), the US (Demargne et al., 2014), Australia (Bennett
46 et al., 2017), and globally (Emerton et al., 2018).

47 The chaotic nature of the atmosphere places a time limit of around 14 days on the
48 predictability of weather from initial atmospheric circulation conditions, although this limit
49 may vary from less than a week to nearly three weeks depending on local climate features
50 and the current weather regime. S2S hydro-meteorological forecasts therefore rely on
51 relatively slowly-varying aspects of the climate system that are more predictable beyond
52 weather time scales, including initial hydro-meteorological conditions and large-scale
53 climate variability modes (Doblas-Reyes et al., 2013; Emerton et al., 2018). . While the skill
54 of seasonal climate forecasts is relatively low in the extra-tropics compared to other parts of
55 the world (Doblas-Reyes et al., 2013), recent progress in forecasting European climate has
56 resulted in skilful seasonal climate forecasts that support various climate services (e.g.
57 Arheimer et al., 2020). For example, the European Flood Awareness System (EFAS) is at the
58 forefront of operational streamflow forecasting in Europe, providing a pan-European service
59 that aims to support preparatory action before major floods. The seasonal component of
60 EFAS uses precipitation, temperature and evaporation from the ECMWF System 5 (SEAS5)
61 seasonal prediction system to drive LISFLOOD, a physics-based distributed hydrological
62 model that estimates hydrological states and fluxes with a daily time step (Arnal et al.,
63 2018). Operationally, EFAS produces seasonal streamflow outlooks for Europe at the
64 beginning of each month up to seven months ahead. Previous work using this setup
65 suggests that skilful forecasts may be obtained for lead times up to one month ahead, but
66 that skill decreases gradually thereafter (Arnal et al., 2018).

67 The conceptual and physics-based hydrological models used operationally are
68 computationally intensive. Spatial downscaling and bias correction are needed to bridge the
69 gap between the relatively coarse spatial scale of S2S climate prediction systems and the
70 finer resolution inputs needed by hydrological models, introducing a layer of methodological
71 uncertainty to the process-based seasonal hydrologic forecasting process. The hydrological
72 forecast outputs may then require further bias-correction before they can be used (Yuan et
73 al., 2015). In contrast, hybrid methods for seasonal streamflow forecasting overcome many
74 of the shortcomings of dynamical approaches (Slater et al. 2023). Instead of using the
75 downscaled outputs of dynamical seasonal prediction systems to drive a hydrological model,
76 hybrid methods use dynamical climate predictions to drive statistical or machine-learning
77 models to directly predict the target variables of interest – e.g. streamflow quantiles or

78 flood frequency. The dynamical climate predictions provide valuable information on large-
79 scale climate patterns and atmospheric conditions, while the statistical or machine-learning
80 models offer the ability to capture complex nonlinear relationships related to streamflow
81 behaviour. Such hybrid approaches follow from similar concepts used in empirical S2S
82 hydrologic prediction, in which observed climate system variables, reanalyses or indices (but
83 not dynamical climate forecasts) are used in statistical schemes to predict streamflow
84 directly (e.g. Mendoza et al., 2017; Regonda et al., 2006).

85 By combining the strengths of both dynamical and statistical approaches, hybrid
86 methods have shown promise for improving seasonal streamflow predictions. For example,
87 Tian et al. (2022) developed a hybrid framework that skilfully predicted month-ahead
88 reservoir inflows in two US watersheds (in Colorado and Alabama) using an ML model driven
89 by seasonal climate forecasts, observed large-scale climate indices and satellite-based
90 estimates of antecedent conditions. In Europe, Hauswirth et al. (2023) showed that a hybrid
91 seasonal forecasting system could skilfully predict surface water level up to three months
92 ahead using ML models driven by climate and hydrological inputs from SEAS5. Hybrid
93 methods are unconstrained by the need to conserve the water balance and implicitly handle
94 biases in the climate data (Slater et al., 2023). Further, they are able to exploit relationships
95 between variables at different spatial and temporal resolutions and spatial extents – e.g.
96 relating daily local streamflow quantiles to monthly climate inputs or large-scale climate
97 patterns (Moulds et al., 2023; Tian et al., 2022).

98 Previous work using observed data has shown that ML models work best when
99 trained on data from multiple catchments (Nearing et al., 2021). While much of the recent
100 literature on this topic focuses on deep learning architectures (e.g. Kratzert et al., 2019),
101 similar results have been found for tree-based models (e.g. Gauch et al., 2021). Multi-site
102 approaches allow the models to learn relationships from a large sample of hydrological
103 variability that encompasses a broad spectrum of catchment characteristics, which they can
104 use effectively to make predictions in individual catchments (e.g. Lees et al., 2021).
105 However, this has not yet been evaluated for seasonal flood prediction using ML models
106 trained on climate forecasts.

107 Here we develop and test a hybrid system to predict the monthly maximum daily
108 flow values (Q_{\max}) at lead times up to four months for 579 catchments in the UK. We train a
109 machine learning model to predict Q_{\max} using seasonal forecasts of precipitation and
110 temperature from the C3S multimodel as well as antecedent conditions and catchment
111 characteristics. We focus on monthly maximum daily streamflow rather than other common
112 S2S hydrologic predictands (e.g., monthly or seasonal average flow) because it serves as an
113 indicator of future flood hazards at S2S lead times, recognizing that individual flood events
114 (timing and magnitude) cannot be skilfully predicted beyond weather time scales. We
115 address two main research questions: (i) How skilfully can we predict monthly maximum
116 daily flow with up to four months lead time using uncorrected monthly dynamical climate
117 forecasts and antecedent conditions? (ii) To what extent can we improve the skill of S2S
118 streamflow predictions at individual sites by developing a multi-site machine learning model
119 that leverages static catchment attributes to learn the hydrological behaviour at individual
120 sites?

121 **2 Materials and methods**

122 **2.1 Data**

123 For the prediction target and observational validation dataset we used daily
124 streamflow observations for Great Britain taken from the National River Flow Archive
125 (NRFA, 2024). We first selected stations that had streamflow records between 1994 and
126 2016 to match the hindcast period of the climate models, before discarding stations with
127 less than 95% data availability in any given year. We also discarded stations that are not
128 included in the CAMELS-GB dataset (Coxon et al., 2020), leaving a total of 579 stations. We
129 computed specific discharge (mm day^{-1}) by dividing the daily streamflow values by the
130 catchment area, then calculated the monthly maximum daily specific discharge for all
131 months and stations.

132 Monthly predictions of precipitation and temperature were obtained from the
133 Copernicus Climate Change (C3S) multimodel seasonal forecasting system. We took
134 seasonal reforecasts (“hindcasts”) of precipitation and temperature for the period 1994-
135 2016 from eight seasonal prediction systems, resulting in a large multimodel ensemble of
136 196 members (Table S1). We computed the multimodel ensemble mean values of
137 precipitation and temperature. We found that including quantiles (0.05, 0.25, 0.5, 0.75,
138 0.95) drawn from the precipitation and temperature ensemble as additional covariates in
139 the ML models did not improve skill (results not shown). All C3S forecasting systems are
140 assigned a nominal start date of the first day of each month such that no members are
141 initialized using observations later than this date, although the initialization method varies
142 across the individual systems. In the text we refer to the predictions for the month
143 immediately following initialization as having a lead time of zero (e.g. for a forecast
144 initialized on August 1st, the zeroth lead time prediction covers August 1-31st). The C3S
145 forecasting system predicts climate up to a minimum of 6 months ahead, but we focus on
146 the first 4 months following initialization as we are unlikely to observe substantial skill for
147 monthly predictands thereafter (e.g. Arnal et al., 2018; Harrigan et al., 2018). We computed
148 the climate inputs for each catchment by taking the area-weighted average monthly value
149 for each variable.

150 We used antecedent mean monthly streamflow as a proxy indicator of initial
151 catchment soil moisture conditions, an important driver of seasonal hydrologic predictability
152 (Arnal et al., 2018; Bierkens & Van Beek, 2009). We used the monthly mean specific
153 discharge in the three months prior to the forecast initialization to create three predictor
154 variables describing the mean specific discharge over one month, two months and three
155 months prior to the nominal forecast initialization date, respectively. We also included
156 estimates of antecedent precipitation using ERA5 reanalysis data, creating variables to
157 represent the average precipitation over one month, two months and three months prior to
158 the initialization time. Antecedent precipitation and streamflow both estimate initial
159 hydrologic condition predictability, and are likely to be colinear predictors, to a degree.
160 However, as random forests are robust to multicollinearity we chose to keep both
161 predictors.

162 Multi-site ML models can benefit from additional information about the catchment
163 characteristics (e.g. Lees et al., 2021, Slater et al., 2024). We added static catchment
164 descriptors from the CAMELS-GB dataset (Table S3; Coxon et al., 2020) to our ML model. We
165 also tried including streamflow signatures that describe the hydrologic behaviour of each
166 catchment, including the baseflow index, slope of the flow duration curve, the 5th and 95th
167 percentile of daily streamflow, and the mean daily streamflow. These were computed using
168 data up to the start of the test period (2004) of our hybrid models, to avoid data
169 contamination (i.e., the situation where a statistical or ML model is inadvertently trained on
170 the same data it will later be tested on). However, although the signature predictors
171 assumed high importance in the QRF model, they did not increase Q_{\max} forecasting skill,
172 suggesting that the model can learn these hydrological characteristics from the static
173 catchment attributes alone. We therefore left out the streamflow signatures from the final
174 multi-site model.

175 **2.2 Methods**

176 We employ quantile regression forests (QRF; Meinshausen, 2006) to predict the
177 monthly maximum of mean daily streamflow (Q_{\max}) using dynamic and static predictor
178 variables. QRFs are a generalisation of random forests (Breiman, 2001) that estimate
179 conditional quantiles from predictor variables, enabling probabilistic predictions of the

180 dependent variable. Like traditional random forests, QRFs are adept at exploiting nonlinear
181 relationships between dependent and independent variables and require relatively little
182 tuning because their performance is less sensitive to the values of hyperparameters than
183 can be the case with other ML methods (Tyralis et al., 2019). QRFs can also be interrogated
184 to establish the relative importance of predictor variables.

185 We train the model directly on the climate forecast outputs to avoid introducing
186 additional uncertainty by performing further post-processing of the dynamical climate
187 forecasts. Similar to other forms of regression, the ML model implicitly performs bias
188 correction by relating the raw climate inputs to observed streamflow (e.g. Slater et al. 2023;
189 Slater and Villarini 2018). We compared three model structures to predict Q_{\max} in each
190 catchment (Table 1). First, we trained QRF models on each streamflow time series
191 independently, giving a site-specific model for every catchment. We compared the single-
192 site models with a multi-site QRF model that was trained on all ($n=579$) available streamflow
193 time series data at once. To assess the extent to which the multi-site model learns from
194 catchment attributes, we also include a multi-site model with the catchment ID as the only
195 static attribute. Owing to the inherent robustness of random forest to potentially irrelevant
196 predictors, whereby unimportant features are automatically assigned low weights, we do
197 not perform predictor variable selection or screening.

198 In both single-site and multi-site approaches, a separate QRF model is trained for
199 each lead time using all months from the training period. This is because the biases in the
200 climate forecasts often change over time from initialization, so a model trained on climate
201 forecasts with a lead time of one month would be unsuitable to make predictions using
202 climate forecasts with a lead time of two months. We note that a similar approach is used
203 for bias correcting seasonal climate forecasts (Crochemore et al., 2016). Thus, for each
204 training period we obtain four models, trained on climate predictions with lead times of
205 one, two, three and four months ahead, respectively. Dataset stratification choices are
206 important in S2S prediction because predictability and prediction system biases typically
207 vary seasonally and with lead time. There are strong geophysical reasons to tailor a
208 statistical or empirical model using both factors, but each stratification dimension reduces
209 the sample size available for training and testing, thus a trade-off is often adopted (e.g.
210 Lehner et al., 2017). Here we do not stratify by initialization date (i.e., season). We

211 construct an ensemble forecast by using the QRF model to predict the conditional quantiles
212 of Q_{\max} corresponding to probabilities between 0.01 and 0.99, with an interval of 0.02.

213 We use a forward-chain cross-validation approach whereby the models are trained
214 on reforecasts from the previous n years and tested on the current year. For example, to
215 predict all months in 2004, the first training period was taken as January 1994 to December
216 2003. For 2005, we then extended the training period by one year to December 2004, and
217 continued adding one year until 2016, the final year in the test period, at which point the
218 training period for the QRF models was January 1994 to December 2015.

219 We evaluated predictive skill using the continuous ranked probability score (CRPS)
220 and associated skill score (CRPSS). The CRPS represents the error between the forecast and
221 observed cumulative distribution functions (Wilks, 2019). It ranges between zero and
222 infinity and is negatively oriented (i.e. smaller values are better), similar in concept to other
223 common error terms (e.g., mean absolute error). We evaluated our forecasts against an
224 observation-based ensemble climatological forecast consisting of the observed monthly
225 streamflow values from the previous 20 years (e.g. Hauswirth et al., 2023). We used the
226 CRPSS to evaluate the skill of our ML forecasts against the reference ensemble climatology.
227 The CRPSS ranges between negative infinity and 1, where 1 indicates perfect skill and 0 or
228 below indicates no skill compared to the reference forecast. We computed the CRPS of the
229 forecast and reference for each month in the test period (2004-2016) and took the mean
230 across individual months to compute the CRPSS.

231 We complemented the CRPS (CRPSS) with the anomaly correlation coefficient (ACC)
232 and reliability index (RI). The ACC varies between -1 and 1, with a score of 1 representing
233 perfect correlation between observed and forecast streamflow values. The RI is a
234 probabilistic measure of the extent to which the forecast ensemble spread represents the
235 uncertainty in observations. It varies between 0 and 1, with 1 denoting a perfectly reliable
236 forecast. Like the CRPSS, we calculate the ACC and RI for every month and lead time
237 separately. Lastly, we assessed the relative importance of the predictor variables using the
238 Gini index, which measures the importance of individual variables in tree-based ML models.
239 Specifically, the Gini index quantifies the extent to which a variable contributes to making

240 homogeneous groups, where outcomes are similar and predictions are more reliable, while
241 reducing impurity, indicating mixed groups with less predictable outcomes.

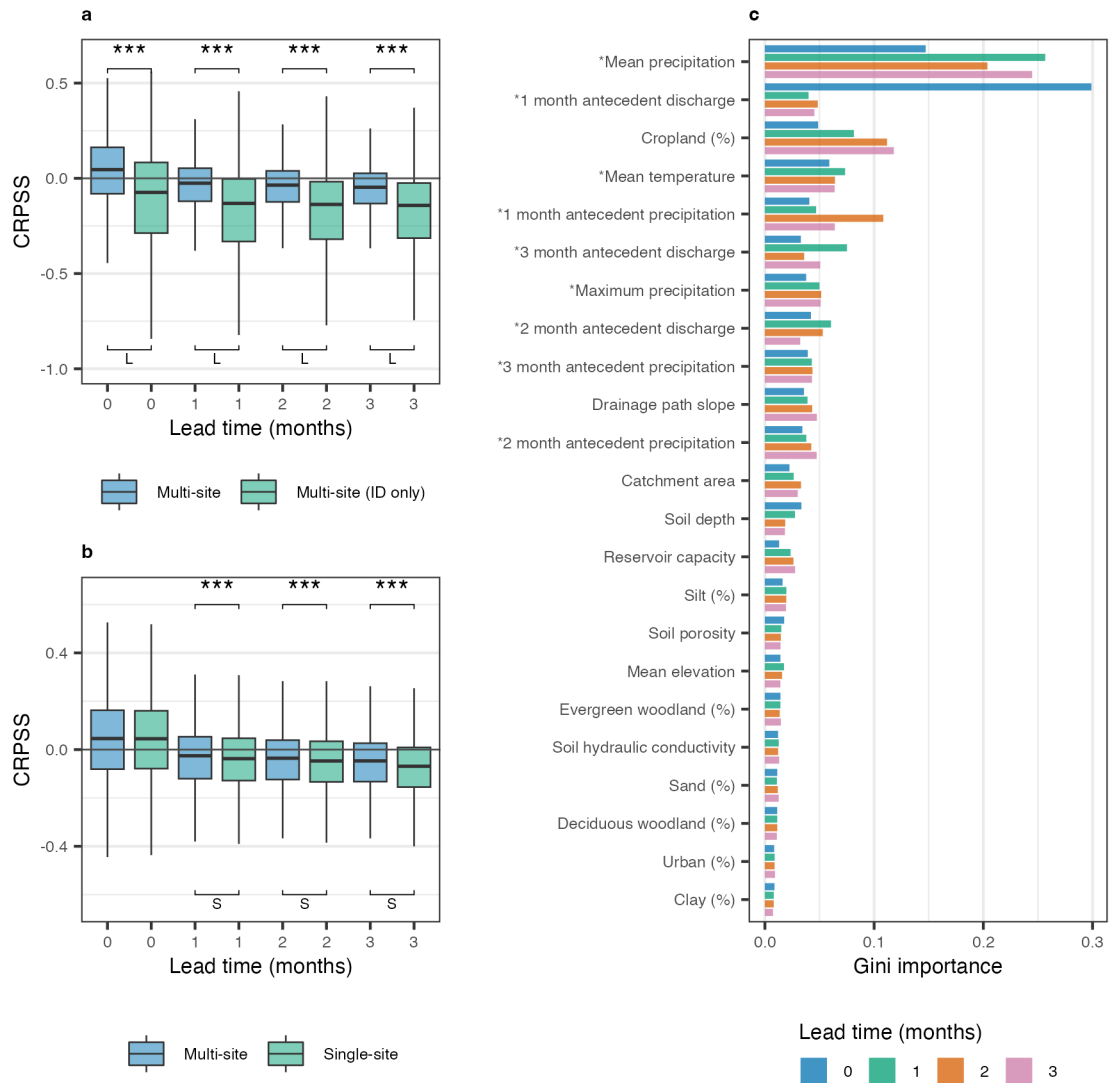
242 **Table 1:** Formulation of the three ML models used in the analysis. Precipitation and
243 temperature are the monthly ensemble mean values from the C3S multimodel system.
244 Antecedent precipitation is the forecasted precipitation from the month prior to the target
245 month, with lead time varying between 1 and 3 months (i.e. to make a prediction in lead
246 time 4 the antecedent precipitation would be taken from lead time 3). Antecedent
247 streamflow is the mean daily observed streamflow prior to the forecast initialization.
248 Catchment attributes are listed in Table S1.

Model name	Configuration	Model description
<i>Single-site</i>	Single-site	Precipitation, temperature, antecedent streamflow and precipitation
<i>Multi-site with ID</i>	Multi-site	Precipitation, temperature, antecedent streamflow and precipitation, catchment ID
<i>Multi-site with attributes</i>	Multi-site	As for single-site model , plus 15 static catchment attributes

249

250 **3 Results**

251 The multi-site model with catchment attributes significantly outperforms the multi-
252 site model with the catchment ID alone (Figure 1a). This suggests that including static
253 catchment attributes enables the model to better reproduce the hydrologic behaviour of
254 different catchments, aligning with previous research for the UK on ML applied to daily
255 streamflow simulation using observed climate inputs (e.g. Slater et al., 2024). Considering
256 the skill scores for each lead time and combining all initialization months, the multi-site
257 model with catchment attributes narrowly but significantly outperforms the single-site
258 models at lead times of one to three months, with a similar average performance between
259 the multi-site and single-site model for the zeroth lead time (Figure 1b). However, the
260 relative performance of the multi-site model with attributes and the single-site model varies
261 by forecast month and lead time (Figure S2). For the zeroth lead time, the multi-site model
262 tends to outperform the single-site model in the months where the highest skill is observed
263 (i.e. December, January, June, July).



264

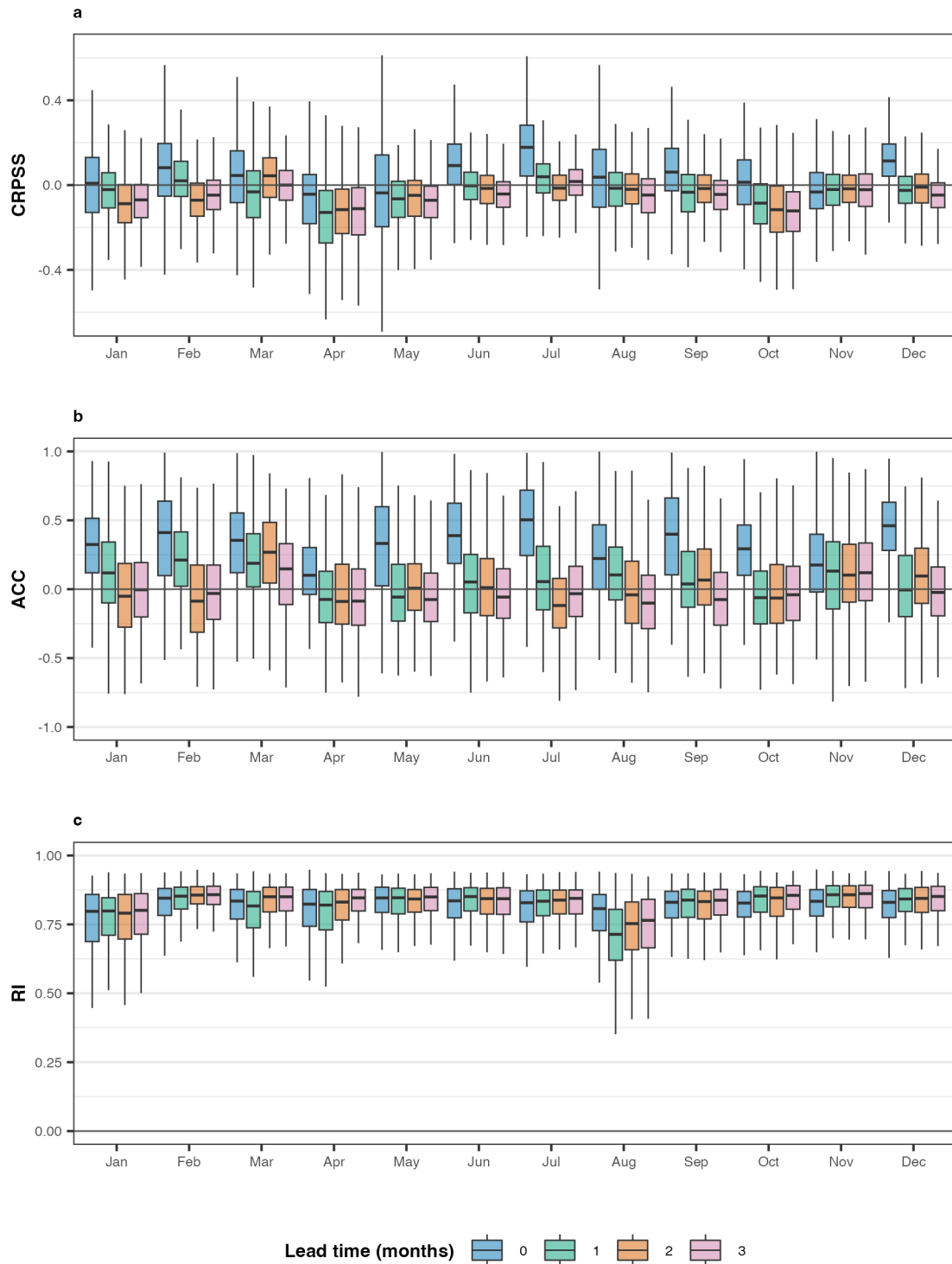
265 **Figure 1:** Analysis of model performance. **a.** Comparison of multi-site models with
 266 catchment attributes and with the catchment ID only. We used a two-sided Wilcoxon signed
 267 rank test to assess whether differences in skill scores between the models were significant
 268 (***) = $p < 0.001$, ** = $p < 0.01$, * = $p < 0.05$). The effect size r is indicated at the bottom of
 269 each plot (S = small effect $0.10 \leq r < 0.3$; M = moderate effect $0.3 \leq r < 0.5$; L = large effect
 270 $r \geq 0.5$). **b.** Comparison of single-site model with multi-site model with catchment attributes.
 271 **c.** Relative importance of predictor variables in the multi-site model with catchment
 272 attributes for each lead time. Time-varying predictors are marked with an asterisk (e.g.
 273 *Mean precipitation).

274

275 We used the Gini index to assess the importance of each predictor variable to the
 276 multi-site model with catchment attributes at each lead time (Figure 1c). Monthly

277 precipitation forecasts have high importance across lead times, while mean temperature
278 forecasts have moderate importance. We included antecedent conditions from observed
279 streamflow and forecast precipitation. Antecedent streamflow is the most important
280 variable at one-month lead time but decreases with importance at later lead times. This is
281 because we are limited to providing antecedent conditions prior to forecast initialization,
282 which has decreasing relevance as the lead time increases, reflecting our general
283 understanding of the influence of initial versus boundary conditions in S2S hydrologic
284 forecasting (e.g. Wood et al., 2016).

285 We assessed skill by computing the monthly CRPSS using a climatological prediction
286 as a reference. We find that there is significant variability in skill during the different months
287 of the year (Figure 2), especially at shorter lead times. For lead time 0, we observed the
288 highest skill in extended winter (DJFM) and late summer (JJAS), with lower skill during spring
289 and autumn. In December and July more than 80% of stations have positive skill in lead time
290 0 (Table 2). In most months, the skill decreases sharply over time, whereas for other months
291 (e.g. March) the skill remains relatively consistent as lead time increases. The variation in
292 skill likely reflects the varying importance of antecedent conditions during the year, as well
293 as the varying skill of the climate forecasts.



294

295 **Figure 2:** Performance assessment of the multisite model with catchment attributes for each
 296 forecast month and lead time. **a.** Continuous ranked probability skill score (CRPSS). We use
 297 climatological forecast as the reference forecast, which is computed separately for each test
 298 year in the simulation. **b.** Anomaly correlation coefficient (ACC). **c.** Reliability index (RI). The
 299 four lead times are shown with different colours.

300 We also compared our results to monthly Q_{\max} drawn from daily EFAS predictions for
301 a subset of the stations included in this study (n=188) that overlapped with the EFAS
302 reference dataset. We bias corrected the EFAS outputs using a quantile mapping approach
303 so that they could be compared with observations. As EFAS outputs daily streamflow
304 estimates we took the maximum daily streamflow prediction from each month and used
305 this value as the reference forecast to estimate CRPSS. Our results are skilful compared to
306 EFAS (Figure S1), and this high relative skill, coupled with the general lack of positive skill of
307 QRF forecast for lead times 1-3 months compared to a climatological reference, indicated
308 that the EFAS predictions were poorer than expected as a benchmark for this particular
309 monthly extreme predictand. We note that our model is specifically trained to predict Q_{\max} ,
310 while EFAS seasonal forecasts are developed for more general purposes, such as supporting
311 tercile probability forecasts for monthly or seasonal mean conditions, a common S2S
312 hydrological product (e.g. Arnal et al., 2018).

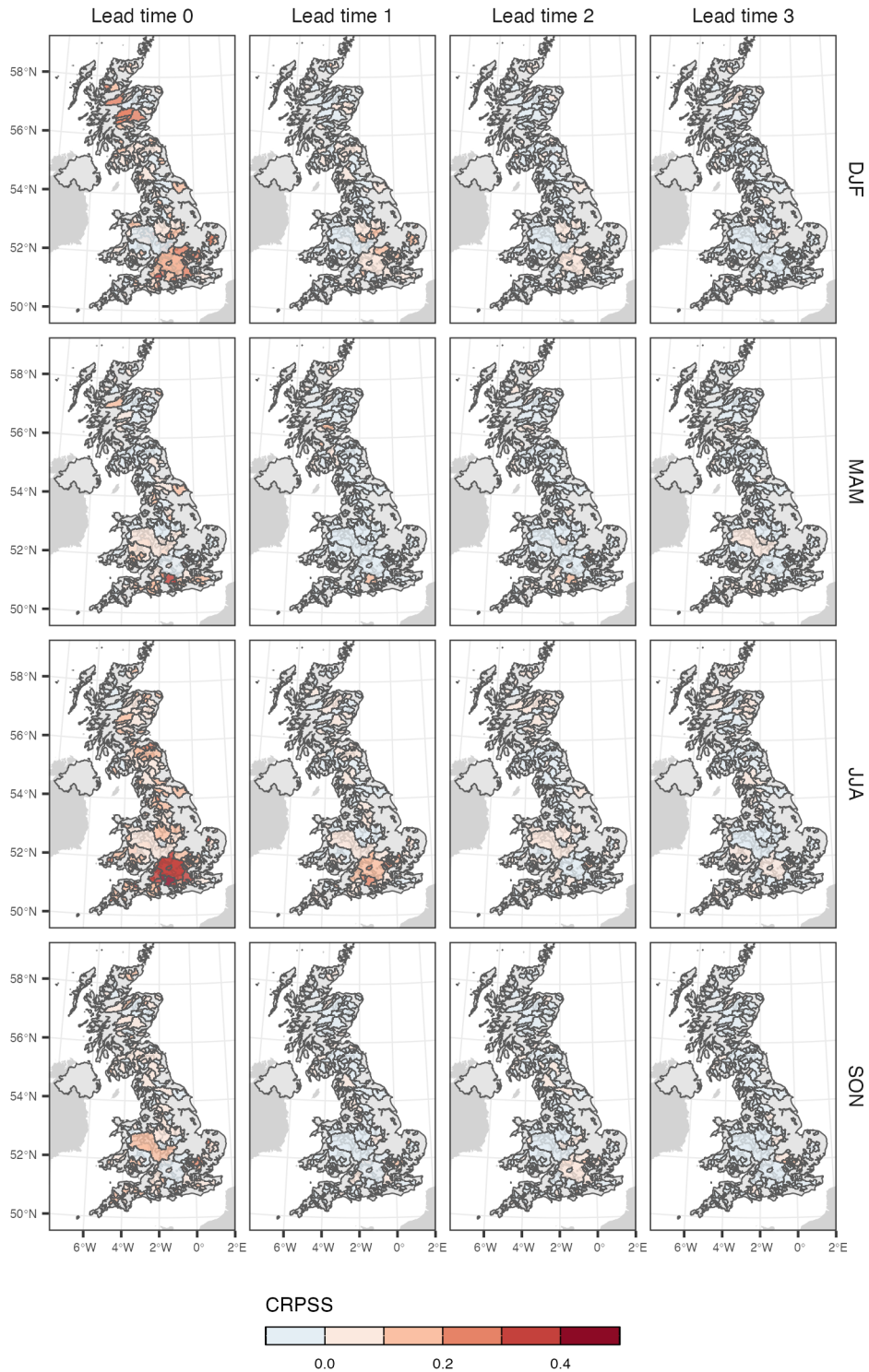
313 As with the CRPSS, the ACC varies by forecast month and lead time (Figure 2b), with
314 the monthly variability in ACC following a similar pattern to that of the CRPSS. In lead time 0,
315 the ACC is positive in >75% of stations across all months. During lead time 1, the ACC is
316 positive in >50% of stations in all months except April, May, and October. Compared to the
317 CRPSS and the ACC the RI is more consistent across months and lead times (Figure 2c).
318 Overall, our ensemble hindcasts have high reliability, with the mean RI across all stations
319 exceeding 0.8 in all months except August.

320 **Table 2:** Percentage of stations (n=579) that are skilful (CRPSS>0) at each lead time and
321 forecast month for the multi-site model with catchment attributes.

Forecast month	Lead time			
	0	1	2	3
January	51.7	42.2	25.3	26.3
February	66.1	59.2	28.0	29.4
March	58.8	42.2	62.3	50
April	38.4	19.2	22.0	20.8
May	46.0	29.8	33.6	24.4
June	76.1	48.3	44.3	31.0

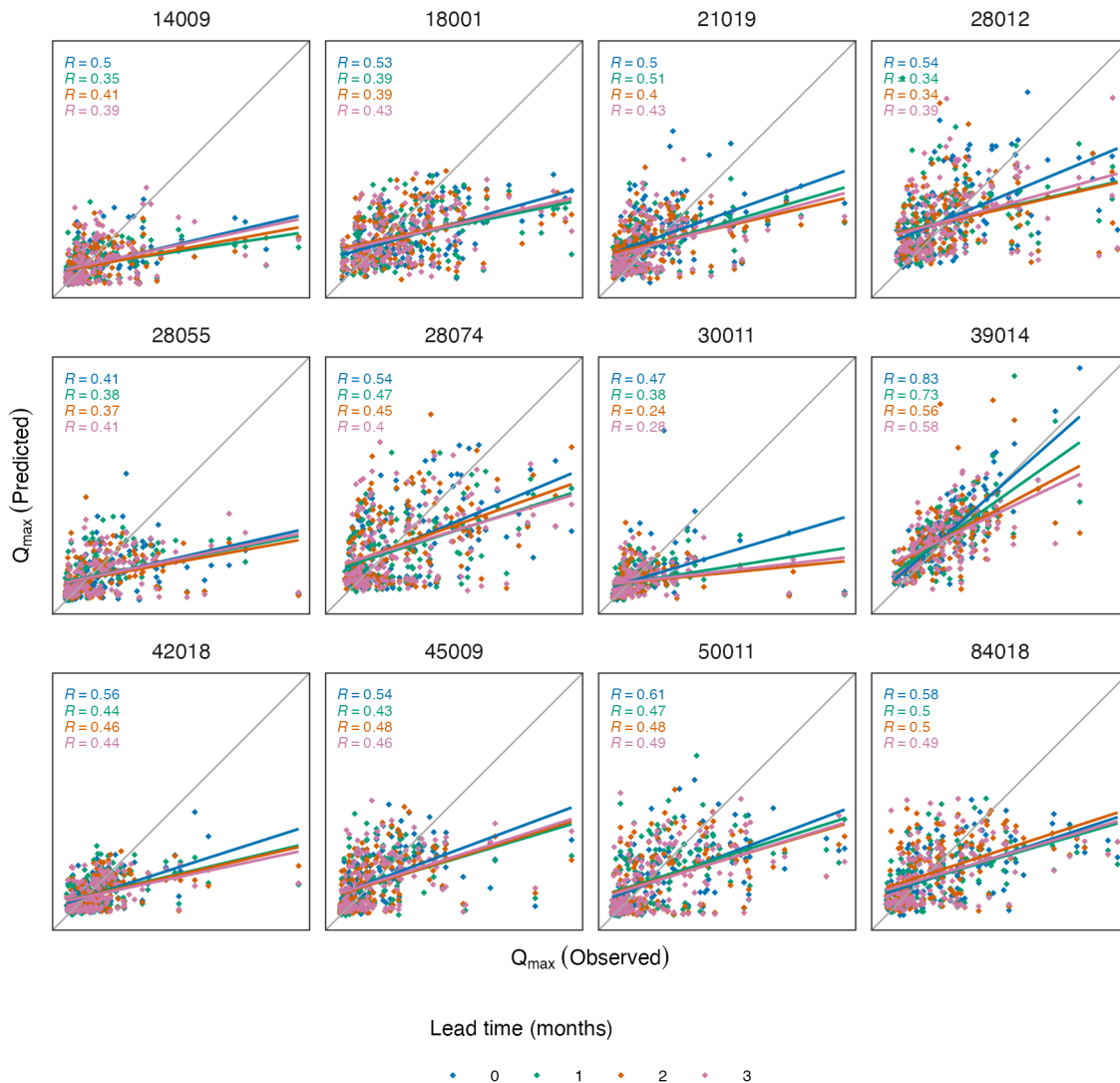
July	81.1	64.5	41.7	59.3
August	56.4	44.3	42.6	33.6
September	67.1	38.2	43.8	31.7
October	53.8	26.6	23.5	18.9
November	40.1	41.3	42.2	42.2
December	83.4	40.0	45.5	28.2

322 We examined the spatial variability in model skill by averaging the monthly skill
323 scores for the multisite model with catchment attributes within each season (Figure 3). At
324 lead time 0 we observe skill in catchments across the UK, while at later lead times, skilful
325 catchments tend to cluster in southern England. This could be related to the location of
326 catchments with relatively slower responding catchments with greater subsurface storage in
327 south-east UK. However, we found relatively weak correlation between ACC and the
328 baseflow index ($R=0.33, 0.31, 0.27, 0.25$ for the four lead times). We observe a tendency for
329 the QRF models to underestimate the observed Q_{\max} , especially the more extreme values
330 (Figure 4). The underestimation is more pronounced as lead time increases, likely due to
331 greater noise in the seasonal climate forecasts at longer lead times.



332

333 **Figure 3:** Average seasonal skill in every catchment by lead time. We calculate the CRPSS per
 334 month and catchment, then compute the seasonal average (DJF, MAM, JJA, SON).



335

336 **Figure 4:** Comparison of observed and predicted Q_{\max} across all months for 12 randomly
 337 selected catchments, by lead time.

338 **4 Discussion**

339 We developed a hybrid forecasting approach for UK flood risk prediction at
 340 subseasonal-to-seasonal time scales using a large multimodel ensemble of climate
 341 predictions. We found that S2S flood predictions are generally skilful (CRPSS>0) up to 1
 342 month following initialization, although skill declines thereafter. However, 90 stations out of
 343 579 retained positive skill in at least three months of the year for all four lead times. Across
 344 all initialization times, 60% of stations show positive skill compared to the climatological
 345 benchmark in the first month after initialization. This drops to 41% in the second month,

346 38% in the third month and 33% in the fourth month. The level of skill varies within the
347 year, with some months generally more skilful than others. This is likely due to a
348 combination of varying climate predictability and the varying importance of antecedent
349 conditions to flood magnitude and frequency during the year. The underlying seasonal
350 forecasts of precipitation and temperature are also most skilful at shorter lead times,
351 although they retain some information at longer lead times.

352 Our work provides guidance on how to build hybrid streamflow prediction systems
353 that combine ML with dynamical climate models. The key finding of our work is the
354 outcome that a multi-site forecast, in which an ML model is trained on data from all
355 catchments at once, tends to outperform single-site model forecasts across all lead times,
356 which aligns with previous work on ML based modelling in hydrology (e.g. Kratzert et al.,
357 2019). However, our work specifically looks at forecasting months ahead, whereas previous
358 work has studied out-of-sample simulation or short-term prediction using observed
359 meteorological or weather forecast inputs. This approach enables the ML model to combine
360 information across time and space into a single model that is trained to discriminate a range
361 of hydrological behaviours. The inclusion of static catchment attributes enables the model
362 to learn the different rainfall-runoff behaviours across the catchments. This is especially
363 important when using ML to predict extremes when training data is limited in time as it
364 means the multi-site model will remain realistic over a larger range of conditions.

365 Hybrid prediction systems require training and testing partitions to evaluate the
366 model performance, and different approaches exist to do this. We implemented a forward-
367 chaining cross validation approach such that the model is never trained on data more recent
368 than the test partition. This reproduces an operational setup as far as possible, where the
369 model is never exposed to information from the future. However, one limitation of this
370 approach for hindcast studies is that the relatively short hindcast period of the C3S
371 multimodel ensemble (i.e. 1994-2016) means the smallest training partition may contain as
372 few as 10 years of monthly data. Nevertheless, during model development we found that
373 increasing the length of the training period by focusing on the predictions from the SEAS5
374 system, which has an extended hindcast period of 1981-2016, did not significantly enhance
375 the performance of the QRF models (results not shown). Moreover, using a multi-site
376 approach reduces the impact of the relatively short reforecast period by pooling data from

377 many catchments to create a much larger training dataset than is used by single-site models
378 (i.e. swapping space for time).

379 Our hybrid seasonal flood forecasts based on eight models from the C3S multimodel
380 ensemble exhibit relatively low skill, as is also the case with traditional (i.e. process-based
381 hydrological model) flood forecasting systems driven by C3S (e.g. Arnal et al., 2018). These
382 findings suggest that the primary constraint on enhanced skill lies in the seasonal climate
383 forecasts. Increasing the skill of climate forecasts is therefore a priority to achieve more
384 useful seasonal streamflow forecasts. One area for further research is to develop ways of
385 identifying ensemble members that are likely to be more skilful over a given time period.
386 Selecting members based on their ability to reproduce large-scale climate patterns such as
387 the NAO is one potential option that has proved successful in other applications (e.g.
388 Dobrynin et al., 2022). Observed climate states, teleconnections and indices (e.g., describing
389 El Nino, the Southern Oscillation, and other climate modes) may be similarly exploited in
390 regions where they exert an influence on weather patterns. These patterns have been
391 deployed in empirical hydrologic forecast systems for many years, while the operational
392 outputs from climate forecast models remain a relatively less-explored source of
393 predictability in hybrid approaches.

394 Operational services for seasonal streamflow forecasts have existed for over a
395 century, offering highly skilled predictions in many parts of the world, and particularly when
396 and where predictors with long persistence are present – such as snowpack or groundwater
397 – as well as strong climate seasonality. Despite their successes, there is growing demand
398 from stakeholders for improved seasonal flow prediction skill at times and in places where it
399 has been more difficult to achieve, usually due to data limitations or hydroclimate
400 considerations. This study illustrates that that a hybrid forecasting approach which is trained
401 over a large-sample collections of watersheds may offer benefits for monthly to seasonal
402 predictions of streamflow. In particular, our approach affords users significant flexibility to
403 define target variables of interest (e.g. Q_{\max}). We use static catchment attributes as
404 predictor variables to allow the QRF model to learn the different relationships between
405 hydroclimate input data and monthly maximum daily streamflow, demonstrating an ability
406 to produce skilful seasonal forecasts of monthly flood risk up to four months ahead in a
407 moderate fraction of the catchments studied. The use of a multi-site ML model that is

408 trained on data from multiple catchments at once may help to alleviate the long-standing
409 problem of small sample sizes when training seasonal predictions on individual sites alone.

410 **Acknowledgements**

411 SM and LJS were supported by UKRI FLF grant MR/V022008/1. LJS was additionally
412 supported by NERC grant NE/S015728/1. AW was supported by the United States Army
413 Corps of Engineers Climate Preparedness and Resilience Program and the United States
414 Bureau of Reclamation Science and Technology Program. The authors would like to
415 acknowledge the use of the University of Oxford Advanced Research Computing (ARC)
416 facility in carrying out this work (<http://dx.doi.org/10.5281/zenodo.22558>) and the UK
417 National River Flow Archive (NRFA) for providing historical daily streamflow time series
418 across Great Britain. We are grateful to Christel Prudhomme, Shaun Harrigan and Michel
419 Wortmann at ECMWF for sharing the latest EFAS reforecasts.

420 **Data availability statement**

421 The input data and scripts that are needed to reproduce the results of this study will be
422 uploaded to a research data repository under an MIT license upon acceptance for
423 publication. They can be made available to reviewers upon request.

424 **References**

- 425 Arheimer, B., Pimentel, R., Isberg, K., Crochemore, L., Andersson, J. C. M., Hasan, A., &
426 Pineda, L. (2020). Global catchment modelling using World-Wide HYPE (WWH), open
427 data, and stepwise parameter estimation. *Hydrology and Earth System Sciences*,
428 24(2), 535–559. <https://doi.org/10.5194/hess-24-535-2020>
- 429 Arnal, L., Cloke, H. L., Stephens, E., Wetterhall, F., Prudhomme, C., Neumann, J., Krzeminski,
430 B., & Pappenberger, F. (2018). Skilful seasonal forecasts of streamflow over Europe?
431 *Hydrology and Earth System Sciences*, 22(4), 2057–2072.
432 <https://doi.org/10.5194/hess-22-2057-2018>

433 Bennett, J. C., Wang, Q. J., Robertson, D. E., Schepen, A., Li, M., & Michael, K. (2017).
434 Assessment of an ensemble seasonal streamflow forecasting system for Australia.
435 *Hydrology and Earth System Sciences*, 21(12), 6007–6030.
436 <https://doi.org/10.5194/hess-21-6007-2017>

437 Bierkens, M. F. P., & Van Beek, L. P. H. (2009). Seasonal Predictability of European
438 Discharge: NAO and Hydrological Response Time. *Journal of Hydrometeorology*,
439 10(4), 953–968. <https://doi.org/10.1175/2009JHM1034.1>

440 Breiman, L. (2001). Random forests. *Machine Learning*, 45(1), 5–32.

441 Coxon, G., Addor, N., Bloomfield, J. P., Freer, J., Fry, M., Hannaford, J., Howden, N. J. K.,
442 Lane, R., Lewis, M., Robinson, E. L., Wagener, T., & Woods, R. (2020). CAMELS-GB:
443 Hydrometeorological time series and landscape attributes for 671 catchments in
444 Great Britain. *Earth System Science Data*, 12(4), 2459–2483.
445 <https://doi.org/10.5194/essd-12-2459-2020>

446 Crochemore, L., Ramos, M.-H., & Pappenberger, F. (2016). Bias correcting precipitation
447 forecasts to improve the skill of seasonal streamflow forecasts. *Hydrology and Earth
448 System Sciences*, 20(9), 3601–3618. <https://doi.org/10.5194/hess-20-3601-2016>

449 Demargne, J., Wu, L., Regonda, S. K., Brown, J. D., Lee, H., He, M., Seo, D.-J., Hartman, R.,
450 Herr, H. D., Fresch, M., Schaake, J., & Zhu, Y. (2014). The Science of NOAA's
451 Operational Hydrologic Ensemble Forecast Service. *Bulletin of the American
452 Meteorological Society*, 95(1), 79–98. <https://doi.org/10.1175/BAMS-D-12-00081.1>

453 Doblus-Reyes, F. J., García-Serrano, J., Lienert, F., Biescas, A. P., & Rodrigues, L. R. L. (2013).
454 Seasonal climate predictability and forecasting: Status and prospects. *WIREs Climate
455 Change*, 4(4), 245–268. <https://doi.org/10.1002/wcc.217>

456 Dobrynin, M., Düsterhus, A., Fröhlich, K., Athanasiadis, P., Ruggieri, P., Müller, W. A., &
457 Baehr, J. (2022). Hidden Potential in Predicting Wintertime Temperature Anomalies
458 in the Northern Hemisphere. *Geophysical Research Letters*, *49*(20).
459 <https://doi.org/10.1029/2021GL095063>

460 Emerton, R., Zsoter, E., Arnal, L., Cloke, H. L., Muraro, D., Prudhomme, C., Stephens, E. M.,
461 Salamon, P., & Pappenberger, F. (2018). Developing a global operational seasonal
462 hydro-meteorological forecasting system: GloFAS-Seasonal v1.0. *Geoscientific Model
463 Development*, *11*(8), 3327–3346. <https://doi.org/10.5194/gmd-11-3327-2018>

464 Gauch, M., Mai, J., & Lin, J. (2021). The proper care and feeding of CAMELS: How limited
465 training data affects streamflow prediction. *Environmental Modelling & Software*,
466 *135*, 104926. <https://doi.org/10.1016/j.envsoft.2020.104926>

467 Harrigan, S., Prudhomme, C., Parry, S., Smith, K., & Tanguy, M. (2018). Benchmarking
468 ensemble streamflow prediction skill in the UK. *Hydrology and Earth System
469 Sciences*, *22*(3), 2023–2039. <https://doi.org/10.5194/hess-22-2023-2018>

470 Hauswirth, S. M., Bierkens, M. F. P., Beijk, V., & Wanders, N. (2023). The suitability of a
471 seasonal ensemble hybrid framework including data-driven approaches for
472 hydrological forecasting. *Hydrology and Earth System Sciences*, *27*(2), 501–517.
473 <https://doi.org/10.5194/hess-27-501-2023>

474 Kratzert, F., Klotz, D., Herrnegger, M., Sampson, A. K., Hochreiter, S., & Nearing, G. S. (2019).
475 Toward Improved Predictions in Ungauged Basins: Exploiting the Power of Machine
476 Learning. *Water Resources Research*, *55*(12), 11344–11354.
477 <https://doi.org/10.1029/2019WR026065>

478 Lees, T., Buechel, M., Anderson, B., Slater, L., Reece, S., Coxon, G., & Dadson, S. J. (2021).
479 Benchmarking data-driven rainfall–runoff models in Great Britain: A comparison of

480 long short-term memory (LSTM)-based models with four lumped conceptual models.
481 *Hydrology and Earth System Sciences*, 25(10), 5517–5534.
482 <https://doi.org/10.5194/hess-25-5517-2021>

483 Lehner, F., Wood, A. W., Llewellyn, D., Blatchford, D. B., Goodbody, A. G., & Pappenberger,
484 F. (2017). Mitigating the Impacts of Climate Nonstationarity on Seasonal Streamflow
485 Predictability in the U.S. Southwest. *Geophysical Research Letters*, 44(24).
486 <https://doi.org/10.1002/2017GL076043>

487 Meinshausen, N. (2006). Quantile Regression Forests. *Journal of Machine Learning Research*,
488 7, 983–999.

489 Mendoza, P. A., Wood, A. W., Clark, E., Rothwell, E., Clark, M. P., Nijssen, B., Brekke, L. D., &
490 Arnold, J. R. (2017). An intercomparison of approaches for improving operational
491 seasonal streamflow forecasts. *Hydrology and Earth System Sciences*, 21(7), 3915–
492 3935. <https://doi.org/10.5194/hess-21-3915-2017>

493 Moulds, S., Slater, L. J., Dunstone, N. J., & Smith, D. M. (2023). Skillful Decadal Flood
494 Prediction. *Geophysical Research Letters*, 50(3), e2022GL100650.
495 <https://doi.org/10.1029/2022GL100650>

496 National River Flow Archive (NRFA) (2024). <https://nrfa.ceh.ac.uk/>. Last accessed: 11th July
497 2024.
498

499 Nearing, G. S., Kratzert, F., Sampson, A. K., Pelissier, C. S., Klotz, D., Frame, J. M., Prieto, C., &
500 Gupta, H. V. (2021). What Role Does Hydrological Science Play in the Age of Machine
501 Learning? *Water Resources Research*, 57(3), e2020WR028091.
502 <https://doi.org/10.1029/2020WR028091>

503 Regonda, S. K., Rajagopalan, B., & Clark, M. (2006). A new method to produce categorical
504 streamflow forecasts. *Water Resources Research*, 42(9), 2006WR004984.
505 <https://doi.org/10.1029/2006WR004984>

506 Slater, L. J., Arnal, L., Boucher, M.-A., Chang, A. Y.-Y., Moulds, S., Murphy, C., Nearing, G.,
507 Shalev, G., Shen, C., Speight, L., Villarini, G., Wilby, R. L., Wood, A., & Zappa, M.
508 (2023). Hybrid forecasting: Blending climate predictions with AI models. *Hydrology
509 and Earth System Sciences*, 27(9), 1865–1889. [https://doi.org/10.5194/hess-27-](https://doi.org/10.5194/hess-27-1865-2023)
510 1865-2023

511 Tian, D., He, X., Srivastava, P., & Kalin, L. (2022). A hybrid framework for forecasting monthly
512 reservoir inflow based on machine learning techniques with dynamic climate
513 forecasts, satellite-based data, and climate phenomenon information. *Stochastic
514 Environmental Research and Risk Assessment*, 36(8), 2353–2375.
515 <https://doi.org/10.1007/s00477-021-02023-y>

516 Tyralis, H., Papacharalampous, G., & Langousis, A. (2019). A Brief Review of Random Forests
517 for Water Scientists and Practitioners and Their Recent History in Water Resources.
518 *Water*, 11(5), 910. <https://doi.org/10.3390/w11050910>

519 Wilks, D. S. (2019). Forecast Verification. In *Statistical Methods in the Atmospheric Sciences*
520 (pp. 369–483). Elsevier. <https://doi.org/10.1016/B978-0-12-815823-4.00009-2>

521 Wood, A. W., Hopson, T., Newman, A., Brekke, L., Arnold, J., & Clark, M. (2016). Quantifying
522 Streamflow Forecast Skill Elasticity to Initial Condition and Climate Prediction Skill.
523 *Journal of Hydrometeorology*, 17(2), 651–668. [https://doi.org/10.1175/JHM-D-14-](https://doi.org/10.1175/JHM-D-14-0213.1)
524 0213.1

525 Yuan, X., Wood, E. F., & Ma, Z. (2015). A review on climate-model-based seasonal hydrologic
526 forecasting: Physical understanding and system development. *WIREs Water*, 2(5),
527 523–536. <https://doi.org/10.1002/wat2.1088>
528

Supplementary materials for Skilful probabilistic predictions of UK floods months ahead using machine learning models trained on multimodel ensemble climate forecasts

This file contains 2 figures (Figure S1—2) and 3 tables (Tables S1—S3)

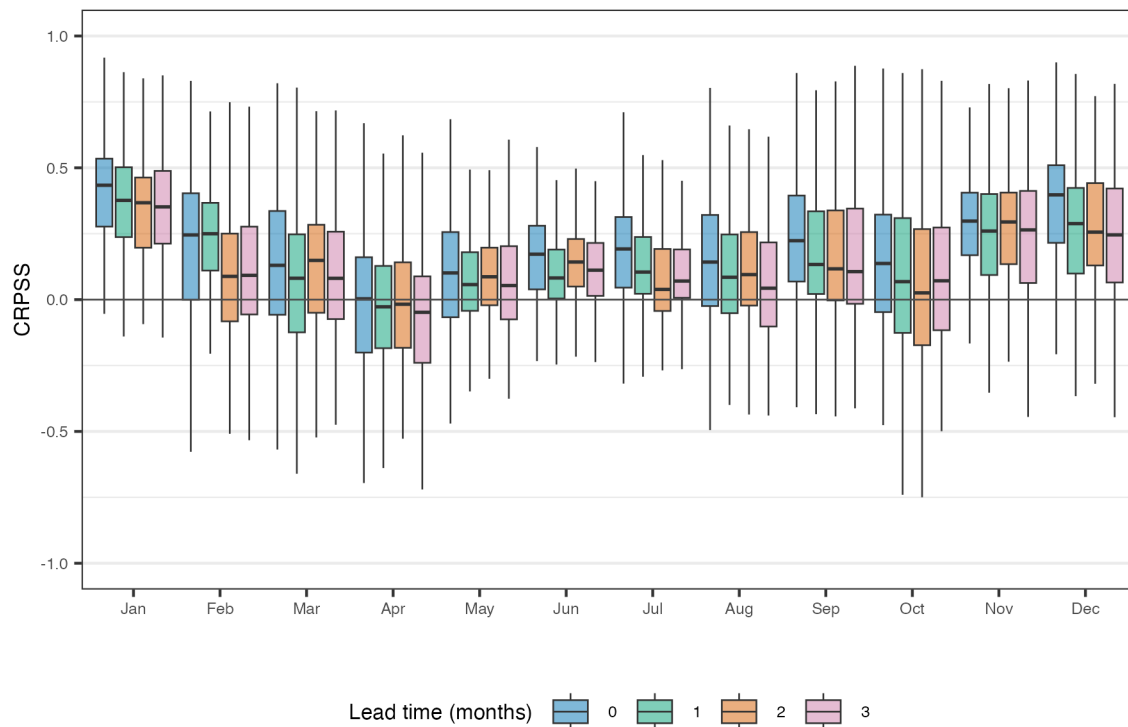


Figure S1: Continuous rank probability skill score of the multisite model with catchment attributes using bias-corrected EFAS hindcasts as a benchmark.

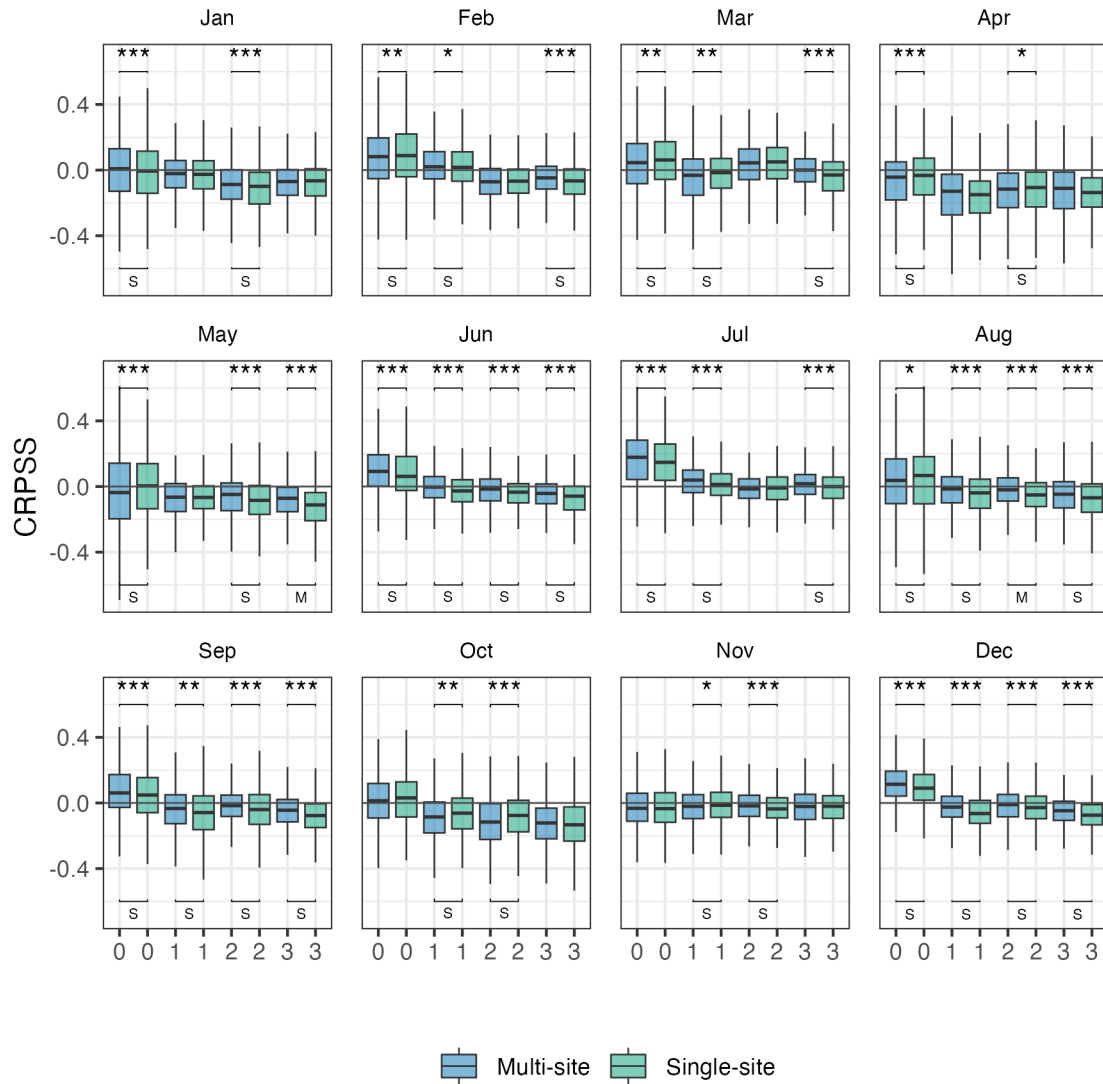


Figure S2: Comparison of CRPSS values for all forecast locations between the single-site model and multi-site model with catchment attributes by month. The skill score used a reference forecast of climatology. We used a one-sided Wilcoxon signed rank test to assess whether differences in skill scores between the models were significant (*** = $p < 0.001$, ** = $p < 0.01$, * = $p < 0.05$). The effect size r is indicated at the bottom of each plot (S = small effect $0.10 \leq r < 0.3$; M = moderate effect $0.3 \leq r < 0.5$; L = large effect $r \geq 0.5$).

Table S1: S2S prediction systems used in the analysis.

Forecast centre	Model	Ensemble size
NCEP	CFSv2	28
CMCC	CMCC-CM2	40
DWD	GCFS2.1	30
ECCC	GEM5-NEMO	10
Met Office	HadGEM3	25
ECMWF	SEAS5	28
Météo-France	System8	25
JMA	CPS3	10

Table S2: Dynamical predictor variables used in the ML models.

Variable	Description
Precipitation	Reforecast precipitation (1994-2016)
Temperature	Reforecast temperature (1994-2016)
Antecedent precipitation	Antecedent precipitation, drawn from forecasts of the month prior to the target month
Antecedent streamflow	Antecedent streamflow, drawn from observations of the month prior to forecast initialisation

Table S3: Static catchment descriptors included in the multi-site model with catchment attributes. Median and range are computed from the subset of 580 basins used in our analysis. All indices were drawn from CAMELS-GB (Coxon et al., 2020). Median and range are given for the 579 catchments included in our study.

Variable	Description	Median	Range
area	Catchment area (km ²)	157	[2, 9931]
elev_mean	Mean elevation (masl)	177	[32, 682]
dpsbar	Slope of the catchment mean drainage path (m km ⁻¹)	86	[11, 488]
sand_perc	Percent sand (%)	43	[19, 86]
silt_perc	Percent silt (%)	30	[9, 42]
clay_perc	Percent clay (%)	23	[4, 50]
porosity_hyres	Soil porosity from hyres pedotransfer function (-)	46	[32, 81]
conductivity_hyres	Soil conductivity from hyres pedotransfer function (cm h ⁻¹)	1.39	[0.60, 3.13]
soil_depth_pelletier	Depth to bedrock (m)	1.23	[0.6, 42]
dwood_perc	Percent cover of deciduous woodland (%)	6	[0, 37]
ewood_perc	Percent cover of evergreen woodland (%)	2	[0, 93]
crop_perc	Percent cover of cropland (%)	10	[0, 88]
urban_perc	Percent cover of urban (%)	3	[0, 83]
reservoir_cap	Reservoir capacity (ML)	0	[0, 8×10 ⁷]